16th World Congress in Computational Mechanics (WCCM)
21-26 July 2024, Vancouver, Canada
A. Korobenko, M. Laforest, S. Prudhomme, R. Vaziri (Eds)

MULTISCALE MODELING OF HYDROGEN TRANSPORT IN STEELS AND ITS RESULTING EMBRITTLEMENT EFFECT

GUANYUE RAO[1], CHUANSHI HUANG[2], AND XIAOSHENG GAO[3]

[1]University of Akron
302 E Buchtel Ave, Akron, OH 44325
gr32@uakron.edu

[2]University of Akron
302 E Buchtel Ave, Akron, OH 44325
ch99@uakron.edu

[3]University of Akron
302 E Buchtel Ave, Akron, OH 44325
xgao@uakron.edu

Key words: Hydrogen Embrittlement, HELP, HEDE, Molecular Dynamics, Phase Field

Abstract. A multiscale modeling approach is adopted in this study to understand the hydrogen embrittlement (HE) mechanisms and to predict failure of engineering components under the influence of hydrogen environment. Molecular dynamics simulations of the body-centered cubic (BCC) iron are conducted to examine the theories of hydrogen enhanced localized plasticity (HELP) and hydrogen enhanced decohesion (HEDE). It is shown that hydrogen aggregation at the crack tip and along grain boundary (GB) reduces the surface energy for creating new crack surfaces, leading to changes in fracture modes caused by preemptive crack propagation. At the continuum level, a numerical framework is developed, which incorporates hydrogen transport in steels and the resulting HELP and HEDE mechanisms into a finite element phase field model to predict crack initiation and propagation in engineering components. As an example, a compact tension (CT) specimen made of a pipeline steel is analyzed. The numerical model captures the phenomenon of hydrogen aggregation occurring proximal to the crack tip driven by the high gradient of hydrostatic stress and large plastic deformation in this region. The resultant hydrogen concentration elicits an interplay of HELP and HEDE effects and reduces the specimen's load carrying capacity. With properly chosen model parameters, the numerical model has the potential of serving as tool for predicting crack propagation and ductile to brittle transition due to the presence of hydrogen.

1 INTRODUCTION

A wide variety of metals, such as steel, aluminum, nickel, and titanium, exhibit a reduction in strength and ductility due to the absorbed hydrogen atoms diffusing into the material during the manufacturing process and/or exposure to the hydrogen environment. This phenomenon is known as hydrogen embrittlement (HE), which is a complex process involving a number of

distinct contributing micro-mechanisms, such as hydrogen enhanced localized plasticity (HELP), hydrogen decreased dislocation emission, hydrogen enhanced decohesion (HEDE), hydrogen induced phase transformation, and stress-induced hydride formation and cleavage. Molecular dynamic (MD) simulation provides a means to reveal the behavior of hydrogen atoms in the material and their effects on crack initiation and propagation. Matsumoto et al. [1] found both HELP and HEDE mechanisms were in action when pre-cracked α-Fe single crystals containing hydrogen were under mode I loading. Hydrogen atoms trapped at the dislocation cores reduced the energy barrier for dislocation motion and increased dislocation mobility, and fracture due to separation of the slip plane was caused by hydrogen atoms trapped by dislocations. On the other hand, Song and Curtin [2] observed that hydrogen atoms in α-Fe aggregated near the crack surface and formed a hydride phase, which prevented dislocation emission, leading to a brittle fracture behavior. Tehranchi [3] observed that interstitial hydrogen atoms prevented dislocation emission and movement. Jung et al. [4] studied the behavior of hydrogen on symmetric tilt grain boundaries (GB) and suggested that both HELP and HEDE contributed to GB separation while the transition from the trans-granular fracture to inter-granular fracture was dominated by the HEDE effect. Xie et al. [5] demonstrated that when a pre-cracked single crystal aluminum was exposed to the hydrogen environment and subjected to loading, dislocations emitted from the crack tip would pile up and form a low angle grain boundary (LAGB). The LAGB would then trap more hydrogen, leading to its cohesive strength substantially reduced and thus entailing a much higher cracking propensity. The insights gained from these MD simulations are inspiring for understanding the HE mechanisms, paving the way for the development of effective strategies to mitigate the detrimental effects of HE on material integrity and performance.

Engineering applications involve length and time scales much larger than those that can be dealt with in MD simulation, and therefore a top-down approach at the continuum level becomes compulsory. There have been various numerical methods developed to predict crack propagation in structural materials, among which the phase field method has a number of appealing advantages such as no need to predefine crack path and its mesh-independent predictions. Miehe et al. [6] introduced a thermodynamically consistent framework for phase field models of crack propagation in elastic solids and proposed a method to implement the phase field model using an operator split algorithm that incrementally updates the fracture phase field and the displacement field. They later extended the model to ductile fracture by adding the non-elastic contribution to the crack driving force defined based on elastic and plastic work densities and barrier functions related to critical values of the inelastic state variables [7]. Huang and Gao [8] proposed a phase field model to simulate both brittle and ductile fracture, in which a degradation function for the yield surface was introduced and the crack driving force was modified to include the plastic contribution. The phase field method offers the advantage of flexibility in implementation and has been successfully applied to simulate various fracture phenomena, providing a versatile tool for investigating hydrogen embrittlement mechanisms in metallic materials. Huang and Gao [9] extended the phase field model they proposed earlier [8] by incorporating hydrogen transport and the resulting HELP and HEDE effects into the governing equations and demonstrated its capability of predicting crack propagation in structural materials under the influence of hydrogen.

In this study, multiscale simulations are conducted to understand the HE mechanisms and to predict failure of engineering components in hydrogen environment. The body-centered cubic

(BCC) iron is considered in the MD simulations, in which the movement of hydrogen atoms and the resulting change of material behavior are studied. The influence of GB is also examined. In the continuum modeling, the phase field method is employed, and the effect of hydrogen on the fracture behavior of a pipeline steel is demonstrated with a compact tension (CT) specimen.

2 MOLECULAR DYNAMICS SIMULATION

2.1 Methods

Ackland et al. [10] developed the interatomic potential for BCC Fe in the format of embedded atom model (EAM). Ramasubramaniam et al. [11] introduced hydrogen interaction into the model, which is further modified by Song and Curtin [2]

$$U = \frac{1}{2}\sum_{\substack{i,j=1 \\ i\neq j}}^{N} \phi_{ij}(r_{ij}) + \sum_{j=1}^{N} F_j\left[\sum_{\substack{i,j=1 \\ i\neq j}}^{N} \rho_{ij}(r_{ij})\right] \tag{1}$$

where ϕ_{ij} is the pair-wise potential, F_j is the embedding function, ρ_{ij} is the density function, and *i* and j are source atom and target atom respectively.

The pair-wise potentials are described as

$$\begin{aligned}
\phi_{FeFe}(r_{ij}) &= \sum_{i=1}^{N^{\phi}} a_i(r-r_i)^{n_i}H(r_i-r)H(r-r_2) + H(r_2-r)H(r-r_1)e^{B_0+B_1r+B_2r^2+B_3r^3} \\
&\quad + \frac{Z_iZ_j{q_e}^2}{r}\Phi\left(\frac{r}{r_s}\right) \\
\phi_{FeH}(r_{ij}) &= \begin{cases} \dfrac{Z_{Fe}Z_H{q_e}^2}{r}\Phi\left(\dfrac{r}{r_s}\right), & \text{for } r < r_1 \\ e^{B_0+B_1r+B_2r^2+B_3r^3+B_4r^4+B_5r^5}, & \text{for } r_1 \le r \le r_2 \\ \sum_{i=1}^{N^{\phi}} {a_i}^{\phi}\left({r_i}^{\phi}-r\right)^3 H({r_i}^{\phi}-r), & \text{for } r > r_2 \end{cases} \\
\phi_{HH}(r_{ij}) &= \begin{cases} s(r)\left(E_{mol}(r) - 2F_H(\rho_H(r))\right) + \left(1-s(r)\right)\left(C_1 f_{cut}(r) + C_2\rho_{HH}(r)\right), & \text{for } r \le r_{cut} \\ 0, & \text{for } r > r_{cut} \end{cases}
\end{aligned} \tag{2}$$

where Z_{Fe} and Z_H are the atomic numbers of the corresponding Fe or H atoms, $q_e$is the electronic charge, H(.) is the Heaviside function, r_s is the screening length, a_0 is the Bohr radius, and $\Phi(x) = 0.1818e^{-3.2x} + 0.5099e^{-0.9423x} + 0.2802e^{-0.4029x} + 0.02817e^{-0.2016x}$

The embedding functions are given as

$$\begin{aligned}
F_{Fe}(\rho) &= -\sqrt{\rho} + a_2\rho^2 + a_4\rho^4 \\
F_H(\rho) &= \sum_{i=1}^{N^F} {a_i}^F\rho^i
\end{aligned} \tag{3}$$

where the density functions can be described as

$$\rho_{FeFe}(r_{ij}) = \sum_{i=1}^{N^{\rho FeFe}} a_i{}^{FeFe} (r_i{}^{\rho FeFe} - r)^3 H(r_i{}^{\rho FeFe} - r)$$
$$\rho_{FeH}(r_{ij}) = \sum_{i=1}^{N^{\rho FeH}} a_i{}^{\rho FeH} (r_i{}^{\rho FeH} - r)^3 H(r_i{}^{\rho FeH} - r)$$
$$\rho_{HFe}(r_{ij}) = \sum_{i=1}^{N^{\rho HFe}} a_i{}^{\rho HFe} (r_i{}^{\rho HFe} - r)^3 H(r_i{}^{\rho HFe} - r) \quad (4)$$

$$\rho_{HH} = \begin{cases} C_{\rho_{HH}} r^2 e^{-\frac{2r}{a_0}} f_{cut}(r) + C_0 \left(\frac{r_{ij} - r_0}{\lambda}\right)^{k-1} e^{-\left(\frac{r_{ij}-r_0}{\lambda}\right)^k - B_0(r_{ij}-r_1)^2}, & \text{for } r_{ij} \geq r_1 \\ C_{\rho_{HH}} r^2 e^{-\frac{2r}{a_0}} f_{cut}(r) + C_0 \left(\frac{r_{ij} - r_0}{\lambda}\right)^{k-1} e^{-\left(\frac{r_{ij}-r_0}{\lambda}\right)^k}, & \text{for } r_2 \leq r_{ij} < r_1 \\ C_{\rho_{HH}} r^2 e^{-\frac{2r}{a_0}} f_{cut}(r), & \text{for } r_{ij} < r_2 \end{cases}$$

Molecular dynamic simulations are conducted using LAMMPS to observe the mechanical behavior of BCC iron under the influence of hydrogen. Two cases are considered in this study: case 1 considers an α-Fe single crystal containing a mode I crack with the initial crack forward direction of [1 1 1] and crack plane normal of [1 -1 0], and case 2 considers a bi-crystal α-Fe containing a Σ5 <100> symmetric tilt GB with an initial crack along the grain boundary. Figure 1 shows the dimensions of the simulation domain. According to deCelis [12], cleavage is most prevalent at [100] planes in cubic systems. A larger angle between the crack direction and the representative cleavage fracture direction would lead to crack tip blunting, leading to plastic deformation before crack propagation.

The simulation is conducted under canonical (NVT) ensemble at 300K over a cylindrical domain with a radius of 150 angstroms and thickness of 14 angstroms with the crack tip at the center. Several layers of atoms are removed to create the initial crack. A boundary layer of 10 angstroms wide surrounding the simulation region is defined and the plane strain, mode I displacement field, as given in Eq. (5), is assigned to the atoms in the boundary layer.

$$u = \frac{K_I}{G}\left(\frac{r}{2\pi}\right)^{\frac{1}{2}} \cos\frac{\theta}{2}\left[1 - 2\nu + \sin^2\frac{\theta}{2}\right]$$
$$v = \frac{K_I}{G}\left(\frac{r}{2\pi}\right)^{\frac{1}{2}} \sin\frac{\theta}{2}\left[2 - 2\nu - \cos^2\frac{\theta}{2}\right] \quad (5)$$

where u and v are the displacements along the initial crack direction and the crack opening direction respectively, the displacement in the thickness direction, *w*, is set to zero for all atoms due to the plane strain condition, K_I represents the mode I stress intensity factor, G is the shear modulus and ν is the Poisson's ratio.

A preload of $K_I = 0.9\text{MPa}\sqrt{\text{m}}$ is first applied to the system to create a hydrostatic stress concentration region to attract hydrogen atoms toward the crack tip. Next, hydrogen atoms are added into the randomly selected interstitial sites incrementally, and each increment is followed by an equilibrium phase of 4 ns. After the desired hydrogen concentration is achieved, the displacement loading is imposed on the boundary layer incrementally. During the loading phase, each increment consists of 8 ps of loading with a loading rate $\dot{K}_I = 5\text{MPa}\sqrt{\text{m}}/\text{ps}$, followed by 2 ns of equilibration.

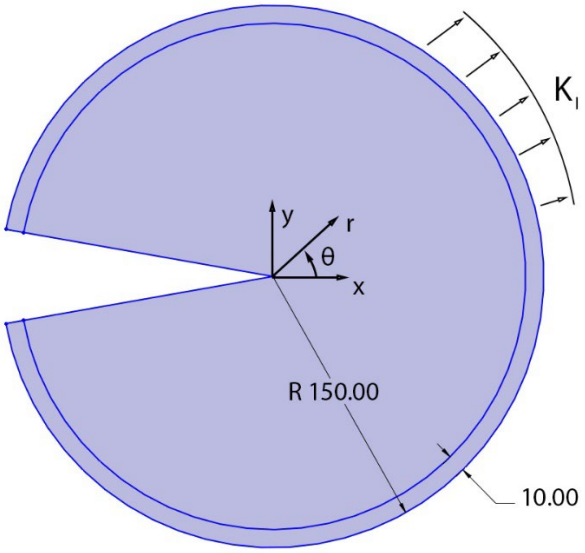

Figure 1. Simulation domain (length unit: Å)

2.2 Results

Figures 2(a) and 2(b) show the effect of hydrogen on the fracture behavior of the α-Fe single crystal under mode I loading. In Fig. 2(a), dislocations emit in the crack tip region, leading to plastic deformation and ductile fracture. With the presence of hydrogen as shown in Fig. 2(b), however, hydrogen atoms tend to aggregate at the crack surface, altering the surface energy dynamics. This aggregation results in a reduction of the surface energy for creating new crack surfaces, ultimately leading to a transition from ductile to brittle fracture behavior.

Figures 2(c) and 2(d) compare the fracture behavior of a bi-crystal α-Fe system with and without the presence of hydrogen. In Fig. 2(c), intragranular cleavage fracture occurs at the preferred lattice plane. However, as shown in Fig. 2(d), the presence of hydrogen atoms introduces additional complexities to the crack propagation process. At grain boundaries, hydrogen atoms occupy imperfection sites, effectively lowering the grain boundary energy. Consequently, crack propagation along the grain boundary is facilitated and promoted.

The observations are summarized in table 1. It is worth mentioning that the different fracture behaviors shown in Figs. 2(a) and 2(c) for single crystal and bi-crystal respectively are primarily because the angle between the initial crack and the preferred lattice plane for cleavage fracture is different for these two cases. More case studies are currently undertaken with different values of such angle.

These observations underscore the impact of hydrogen atoms on the behavior of crack propagation in metallic materials. This understanding of the hydrogen-induced alterations in crack propagation behavior is crucial for elucidating the mechanisms of hydrogen embrittlement in metals. The simulations presented above show that hydrogen atoms reduce cohesion energy between Fe atoms and also prevent dislocation formation and movement, thus promoting ductile-to-brittle transition. But Sofronis and Robertson[13] observed that hydrogen atoms decrease stacking fault energy and enable dislocation movement. Further investigations are needed to resolve this discrepancy.

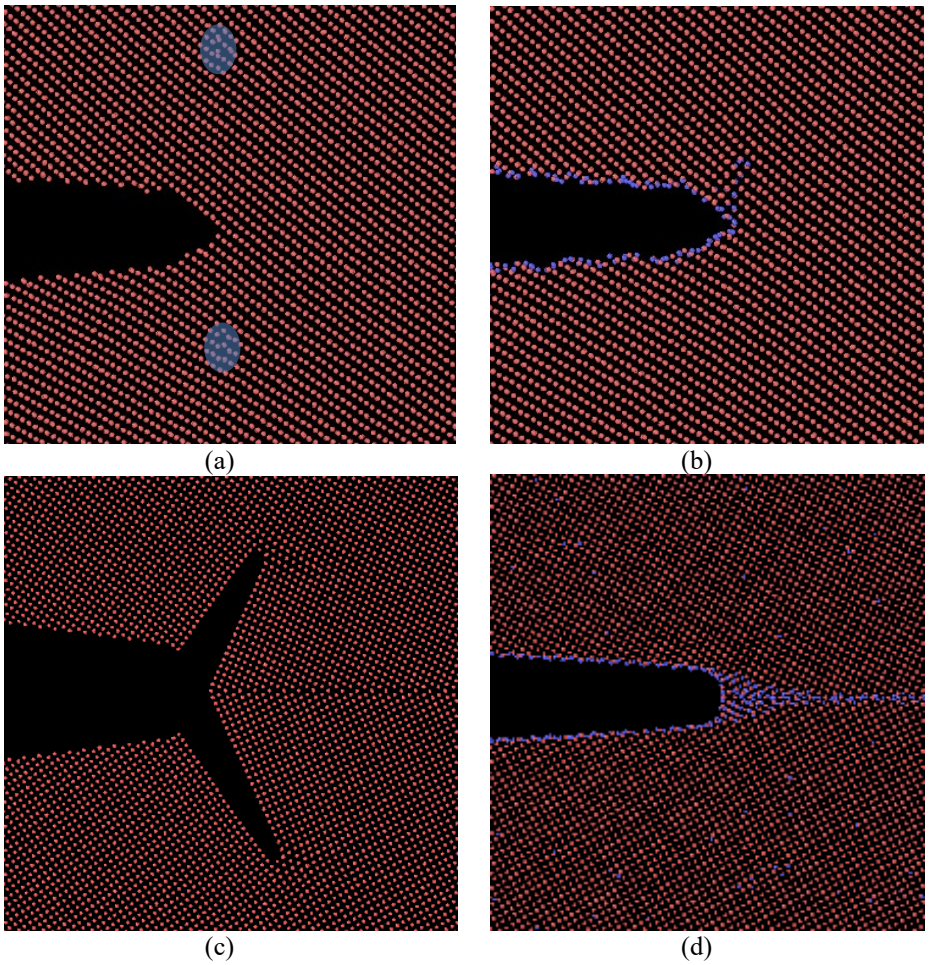

Figure 2. Behavior of various molecular systems under mode I loading: (a) plastic deformation of single crystal Fe, highlighted regions mark the dislocation emission, (b) cleavage crack along lattice direction of sing crystal Fe with presence of hydrogen atoms, (c) intragranular cleavage crack of bi-crystal Fe, and (d) intergranular crack along GB with presence of hydrogen atoms

Table 1. Crack behaviors under mode I loading

	without H presence	**with H presence**
Single-crystal	Plastic deformation	Cleavage crack
Bi-crystal	Intragranular cleavage crack	Intergranular crack along GB

3 CONTINUUM MODEL WITH THE PHASE FIELD METHOD

3.1 Phase Field Method

In the phase field method, the fracture surface is represented by a phase field variable d ($0 \leq d \leq 1$), where $d = 0$ denotes a completely intact state of the material and $d = 1$ denotes a fully broken state. The crack in the phase field model is diffusive and a length scale, l, is introduced. The degradation function used to describe the continuously broken process of the material is defined as $g(d) = (1 - d)^2$, and both the Young's modulus and the yield surface are assumed

to deteriorate with the increasing phase field value. Huang and Gao [8] introduced a modified crack driving force

$$\widetilde{H} = \frac{\Psi^{e+}}{G_c / l\, A} \tag{6}$$

where Ψ^{e+} is the stored elastic energy density due to the deviatoric stress and the tensile part of the volumetric stress, G_c is related to fracture energy, and A is a plastic adjustment function expressed as

$$A = \exp\left(\frac{\alpha \varepsilon_p}{\varepsilon_f}\right) \tag{7}$$

in which ε_p represents the equivalent plastic strain, ε_{f} is related to material failure strain and α is an adjustment factor. In the numerical examples presented in this section, G_c is taken as 100 kJ/m^2, ε_{f} is taken as 0.1, and α is taken as 0.5.

3.2 Hydrogen Transport in Steels

The dissolved hydrogen is assumed to reside either at normal interstitial lattice sites (NILS) or trapping sites generated by plastic deformation, and the two populations are assumed to be in equilibrium according to Oriani's theory [14]. Huang and Gao [10] derived the governing equation of hydrogen diffusion that is coupled with deformation and phase field as follows

$$\frac{C_L + C_T(1-\theta_T)}{C_L}\dot{C}_L - \nabla\cdot(\overline{D}_L \nabla C_L) + \nabla\cdot\left(\frac{\overline{D}_L C_L V_H}{R\Theta}\nabla\sigma_h\right) + \theta_T \frac{dN_T}{d\varepsilon_p}\dot{\varepsilon}_p = 0 \tag{8}$$

in which C_{L} represents the lattice hydrogen concentration, C_{T} represents the trapped hydrogen concentration, θ_{T} represents the occupancy of the trapping sites, N_{T} represents the trapping site density, which is a function of the plastic strain, $\overline{D}_L$ is the effective diffusion coefficient defined as $\overline{D}_L = (1-d)^2 D_L$, where D_L is the initial hydrogen diffusion coefficient through NILS when material is not damaged and is taken as 0.0127 mm^2/s, σ_h is the hydrostatic stress, ε_p is the equivalent plastic strain, V_H is the partial molar volume of hydrogen, Θ is the absolute temperature, and R is the universal gas constant.

Based on the experimental observations presented by Kumnick and Johnson [15], Taha and Sofronis [16] proposed a trap density function for iron and steels. Adapting to the phase field method, Huang and Gao [10] modified it to an incremental form

$$\log(N_T) = 23.26 - 2.33\exp(-5.5\tilde{\varepsilon}_p) \tag{9}$$

where the unit of N_T is traps/m^3 and the equivalent plastic strain is replaced by an incremental plastic factor $\tilde{\varepsilon}^{\mathrm{p}}$. At time increment $n+1$, the plastic factor is defined as $\tilde{\varepsilon}^{\mathrm{p}}_{n+1} = \tilde{\varepsilon}^{\mathrm{p}}_{n} + (1-d_{n+1})^2 \Delta\bar{\varepsilon}^{\mathrm{p}}$.

3.2 HELP and HEDE Models

Sofronis et al. [17] proposed a simple model to describe the HELP effect by reducing the yield stress with the increase of hydrogen concentration.

$$\sigma_0(C) = f(C)\,\sigma_0, \tag{10}$$

$$f(C) = \begin{cases} (\xi - 1)\dfrac{C}{C_0} + 1 & f(C) > \eta \\ \eta & f(C) \le \eta \end{cases}$$

where C is the hydrogen concentration, σ_0 is the yield stress with no presence of hydrogen, ξ is a softening parameter defining the yield stress when the hydrogen concentration equals to C_0, and η defines the lowest possible value of yield stress, or minimum yield strength.

Huang and Gao [10] proposed a similar model to describe the HEDE effect

$$\tilde{G}_c(C) = g(C)\, G_c \ , \qquad g(C) = \begin{cases} (\zeta - 1)\frac{C}{C_0} + 1 & f(C) > \vartheta \\ \vartheta & f(C) \le \vartheta \end{cases} \tag{11}$$

In the numerical examples presented in this section, ξ and ζ are taken as 0.9, while η and ϑ are taken as 0.5. The initial hydrogen concentration is taken as 2.084×10^{12} atoms/mm^3.

3.3 Numerical Example

The material considered is a pipeline steel having a Young's modulus of 200 GPa and Poisson's ratio of 0.3. The tensile stress-strain curve was fitted into a power-law relation, resulting in $\sigma_0 = 275$ MPa and $N = 0.166$. A compact tension (CT) specimen is simulated with the plane strain condition. Fig. 3(a) shows the finite element mesh of the half model, where 8-node hexahedral elements are used. Fig. 3(b) shows a close-up of the crack tip region. Displacements of all nodes in the thickness direction are fixed and the symmetry condition is imposed on the nodes in the ligament. An initial, uniform hydrogen concentration of 2.084×10^{12} atoms/mm^3 is assumed and all external surfaces are insulated such that there is no hydrogen flux in and out the specimen. A displacement load is applied through the hole.

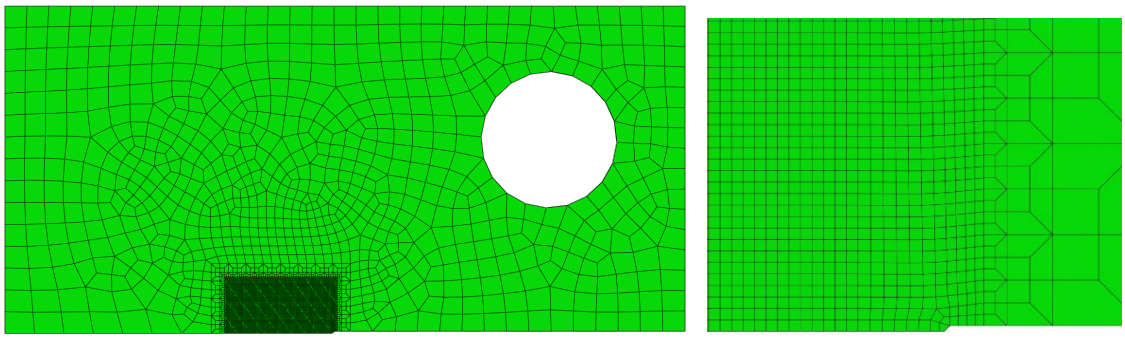

(a) (b)

Figure 3. (a) Mesh of a compact tension specimen (b) close-up of the crack tip region

Figures 4(a-c) illustrate the distributions of the phase field value, hydrostatic stress, and plastic strain respectively at the onset of crack initiation. Figs. 4(d-f) show the corresponding distributions of hydrogen concentration at NILS (C_L), hydrogen concentration at trapping sites (C_T), and total hydrogen concentration ($C = C_L + C_T$). The lattice hydrogen concentration is notably high in the region ahead of the crack tip due to elevated hydrostatic stress. On the other hand, the concentration of trapped hydrogen is prominent in a localized area where plastic deformation occurs at the crack tip.

Figures 5(a-c) illustrate the distributions the distributions of the phase field value, hydrostatic stress, and plastic strain respectively after some amount of crack propagation. Figs. 4(d-f) show the corresponding distributions of C_L, C_T and C. As the crack propagates, the region of high hydrostatic stress moves with the new crack tip. The plastic strain contour behind the new crack

tip is due to the fact that in the phase field model, the crack is diffusive and the fractured elements are not removed.

Figure 6 compares the load-displacement curve of the hydrogen-containing specimen (dashed line) and the one which does not contain hydrogen (solid line). The symbols on the curves indicate the onset of crack initiation. The presence of hydrogen, because of the HELP and HEDE effects, leads to an earlier crack initiation and lower load-carrying capacity of the specimen.

To further obtain the crack resistance curve, the *J*-integral can be computed using the domain integral method [18] or calculated using the load-displacement curve according to ASTM E1152 [19], which can be done without much technical challenges.

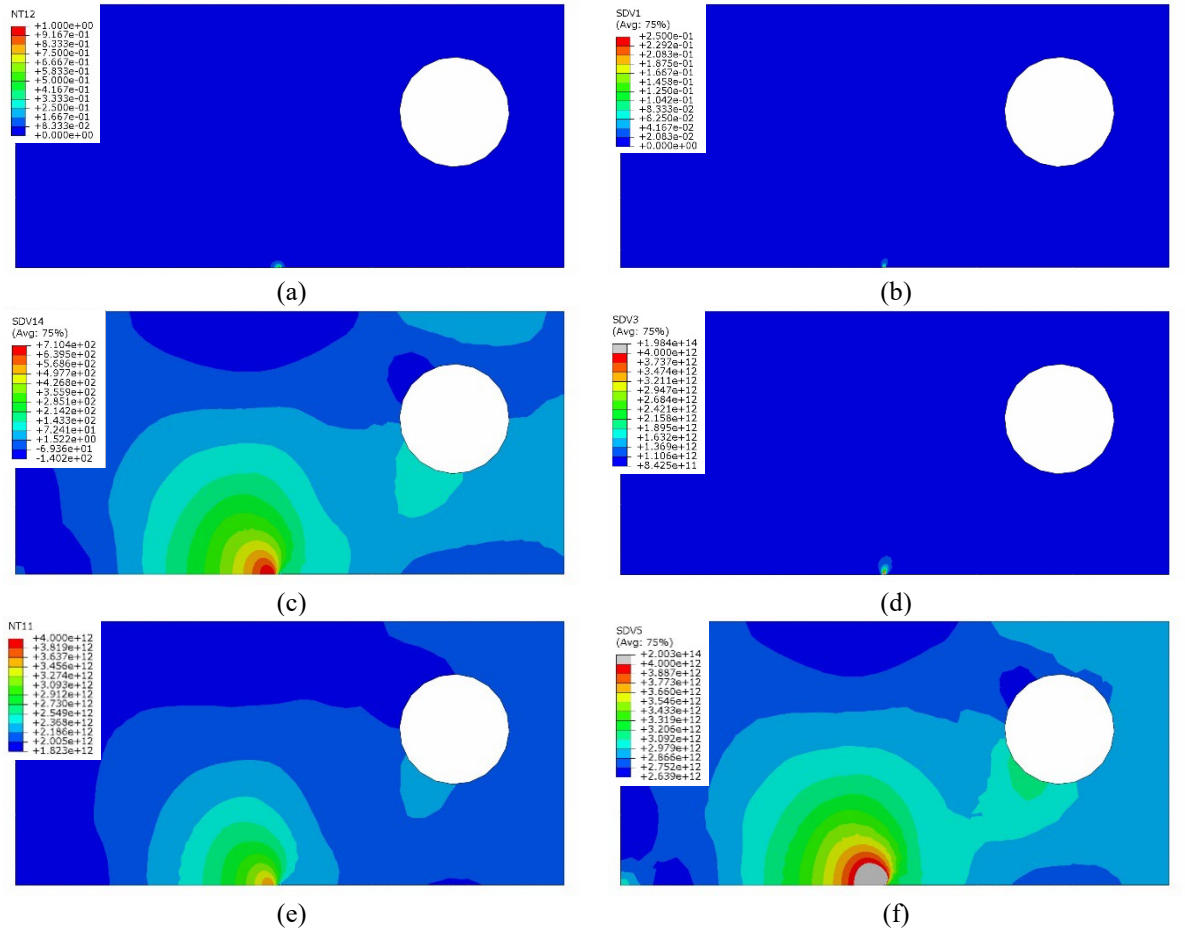

Figure 4. Distributions of (a) phase field value, (b) plastic strain (c) hydrostatic stress distribution, (d) concentration of trapped hydrogen (C_T), (e) concentration of hydrogen at NILS (C_L), and (f) total hydrogen distribution (C) prior to fracture initiation.

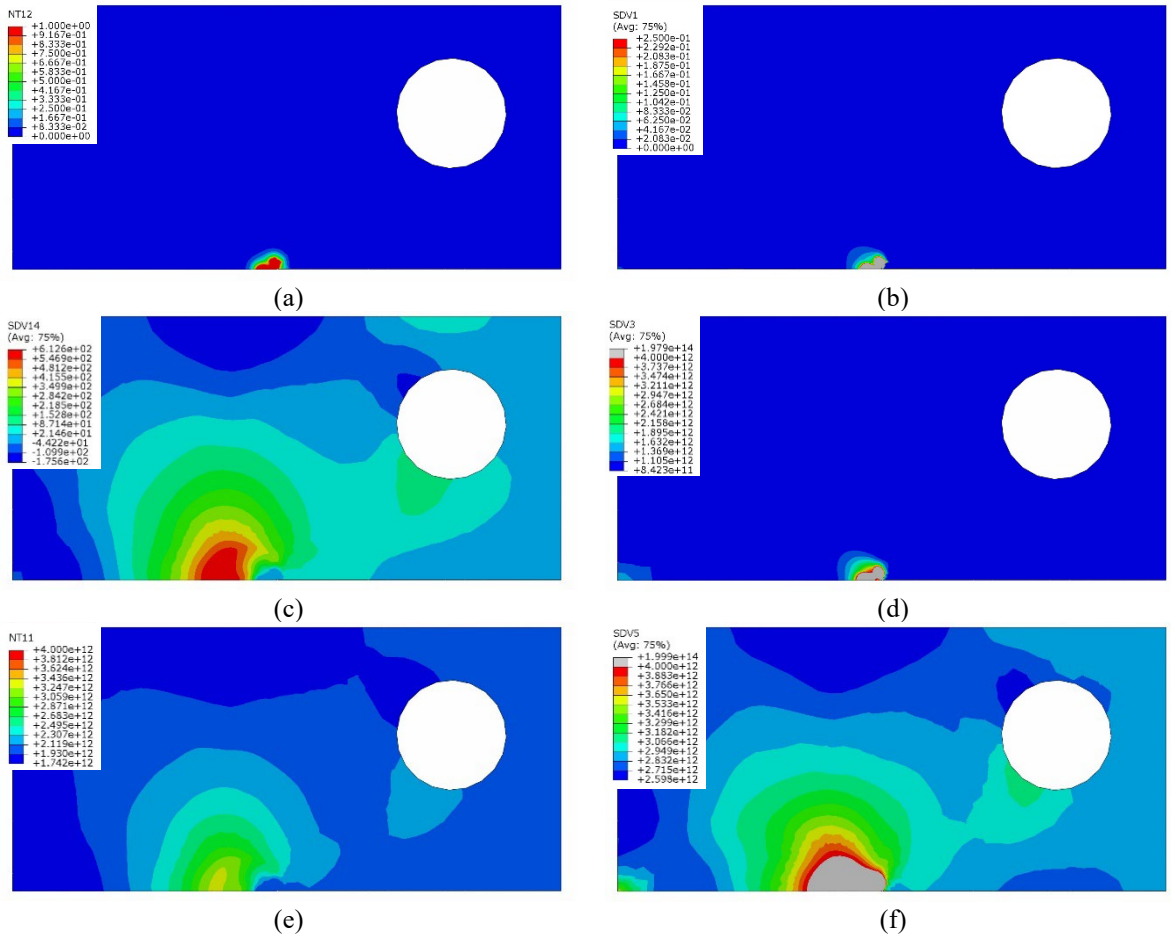

Figure 5. Distributions of (a) phase field value, (b) plastic strain (c) hydrostatic stress distribution, (d) concentration of trapped hydrogen (C_T), (e) concentration of hydrogen at NILS (C_L), and (f) total hydrogen distribution (C) after some amount of crack propagation.

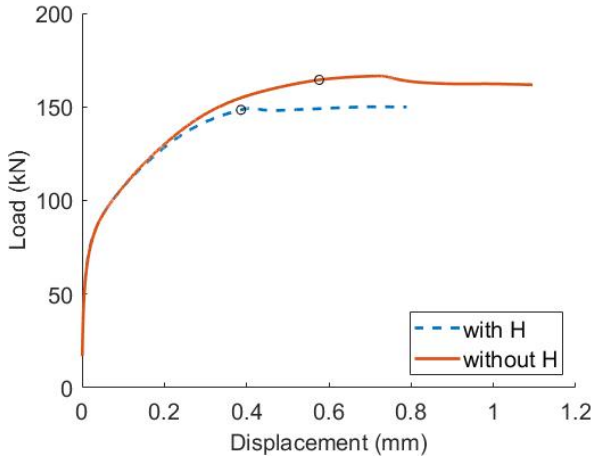

Figure 6. Computed load-displacement curves of the compact tension specimen with and without the presence of hydrogen.

4 Summary

A multiscale modeling investigation is undertaken to study the effects of hydrogen on the fracture behavior of iron and steel. Molecular dynamic simulations are conducted to probe the mechanisms leading to the changes in crack behavior in α-Fe under mode I loading. It is shown that the presence of hydrogen atoms elicited discernible alterations in fracture behavior within the BCC Fe. In single-crystal Fe, the hydrogen-induced reduction in cohesion energy precipitated a transition from ductile to brittle behavior along the slip pane. In bi-crystal Fe, hydrogen atoms aggregate at the grain boundary, which reduces GB energy and promotes crack propagation along GB. Both observations support the theory of HEDE. At the continuum level, a numerical framework is developed, which incorporates hydrogen transport in steels and the resulting HELP and HEDE mechanisms into a finite element phase field model. Simulation results of a compact tension specimen show that hydrogen accumulates at the crack tip region driven by positive hydrostatic stress as well as more traps produced by plastic deformation in this area. This process continues as the crack propagates in the material. The interplay of HELP and HEDE effects decreases the fracture toughness and reduces the load carrying capacity of the specimen. The model shows a promising potential to be used as a numerical tool to predict failure of engineering components in hydrogen environment.

REFERENCES

[1] Matsumoto, R. et al. Atomistic simulations of hydrogen embrittlement. *International Journal of Hydrogen Energy* 34.23 (2009): 9576-9584.

[2] Song, J. and Curtin, W.A. Atomic mechanism and prediction of hydrogen embrittlement in iron. *Nature Materials* 12.2 (2013): 145-151.

[3] Tehranchi, A. and Curtin, W.A. The role of atomistic simulations in probing hydrogen effects on plasticity and embrittlement in metals. *Engineering Fracture Mechanics* 216 (2019): 106502.

[4] Jung, SP. et al. Influence of hydrogen on the grain boundary crack propagation in bcc iron: A molecular dynamics simulation. *Computational Materials Science* 149 (2018): 424-434.

[5] Xie, DG., Wan, L. and Shan, ZW. Hydrogen enhanced cracking via dynamic formation of grain boundary inside aluminum crystal. *Corrosion Science* 183 (2021): 109307.

[6] Miehe, C., Hofacker, M. and Welschinger, F. A phase field model for rate-independent crack propagation: Robust algorithmic implementation based on operator splits. *Computer Methods in Applied Mechanics and Engineering* 199.45-48 (2010): 2765-2778.

[7] Miehe, C., Hofacker, M., Schänzel, L.M. and Aldakheel, F. Phase field modeling of fracture in multi-physics problems. Part II. Coupled brittle-to-ductile failure criteria and crack propagation in thermo-elastic-plastic solids, *Computer Methods in Applied Mechanics and Engineering* 294 (2015) 486–522.

[8] Huang, C. and Gao, X. Development of a phase field method for modeling brittle and ductile fracture. *Computational Materials Science* 169 (2019): 109089.

[9] Huang, C. and Gao, X. Phase field modeling of hydrogen embrittlement. *International Journal of Hydrogen Energy* 45 (2020): 20053-20068.

[10] Ackland, G.J. et al. Development of an interatomic potential for phosphorus impurities in α-iron. *Journal of Physics: Condensed Matter* 16.27 (2004): S2629.

[11] Ramasubramaniam, A., Itakura, M. and Carter, E.A. Interatomic potentials for hydrogen in α–iron based on density functional theory. *Physical Review B* 79.17 (2009): 174101.
[12] Decelis, B., Argon, A.S. and Yip, S. Molecular dynamics simulation of crack tip processes in alpha-iron and copper. *Journal of Applied Physics* 54.9 (1983): 4864-4878.
[13] Sofronis, P. and Robertson, I.M. Transmission electron microscopy observations and micromechanical/ continuum models for the effect of hydrogen on the mechanical behavior of metals. *Philosophical Magazine A* 82.17-18 (2002): 3405-3413.
[14] Oriani, R.A. The diffusion and trapping of hydrogen in steel. *Acta Metallurgica*, 18.1 (1970): 147-157.
[15] Kumnick AJ, Johnson HH. Deep trapping states for hydrogen in deformed iron. *Acta Metallurgica* 28(1980):33–39.
[16] Taha A, Sofronis P. A micromechanics approach to the study of hydrogen transport and embrittlement. *Engineering Fracture Mechanics* 68(2001): 803–37.
[17] Sofronis P, Liang Y, Aravas N. Hydrogen induced shear localization of the plastic flow in metals and alloys. *European Journal of Mechanics - A/Solids* 20 (2001): 857–72.
[18] Shih, C.F., Moran, B. and Nakamura, T. Energy release rate along a three-dimensional crack front in a thermally stressed body. *International Journal of Fracture* 30(1986): 79-102.
[19] ASTM International. E1152-87: *Standard test method for determining J-R curves*. 1990 Annual Book of ASTM standards, Section 3 (1990).